Arabian Journal of Chemistry (2016) **xxx**, xxx–xxx

King Saud University

Arabian Journal of Chemistry

www.ksu.edu.sa
www.sciencedirect.com

ORIGINAL ARTICLE

Oleylamine surface functionalized $FeCo_yFe_{2-y}O_4$ ($0.0 \leqslant y \leqslant 1.0$) nanoparticles

Md. Amir [a,*], **A. Baykal** [b], **H. Sözeri** [c], **H. Güngüneş** [d], **Sagar E. Shirsath** [e]

[a] *Department of Bio & Nanotechnology Engineering, Faculty of Engineering, Istanbul University, 34320 Avcilar, İstanbul, Turkey*
[b] *EYRA Textile Chemicals and Chemical Industry Trade Company, Saraçlar Industrial Zone, No: 3-12, 34490, İkitelli, İstanbul, Turkey*
[c] *TUBITAK-UME, National Metrology Institute, 41470 Gebze, Kocaeli, Turkey*
[d] *Department of Physics, Hitit University, 19030 Çorum, Turkey*
[e] *Spin Device Technology Center, Engineering Faculty, Shinshu University, 380-8553 Nagano, Japan*

Received 20 June 2016; accepted 20 October 2016

KEYWORDS

Magnetic properties;
Fe_3O_4, Co^{3+} substitution;
Oleylamine;
Cation distribution;
Mössbauer analysis

Abstract In this study, oleylamine (OAm) capped $FeCo_yFe_{2-y}O_4$ ($0.0 \leqslant y \leqslant 1.0$) nanocomposites (NCs) were prepared via a polyol route. Effect of Co^{3+} ion substitution on structure, morphology and magnetic properties of Fe_3O_4 nanoparticles was investigated by X-ray diffraction (XRD), fourier transform infrared spectroscopy (FT-IR), thermal gravimetric analyzer (TGA), scanning and transmission electron spectroscopy (SEM and TEM), vibrating sample magnetometer (VSM) and Mössbauer analyzer. All XRD patterns show the single phase spinel ferrite without any impurity. The crystallite size of the samples is within the range of 7.1–21.7 nm. FT-IR analysis showed that all products were successfully packed by OAm. Both SEM and TEM results confirmed that products have spherical morphology with small agglomeration. When Co^{3+} ions were substituted to the Fe_3O_4, Ms continued to decrease up to Co^{3+} content of $y = 0.4$. It was reported that Co^{3+} ions prefer to replace Fe^{2+} ions on octahedral side up to some concentration. Although the Mössbauer spectra for the all samples were composed of magnetic sextets, superparamagnetic particles are also formed for $FeCo_{0.6}Fe_{1.4}O_4$, $FeCo_{0.8}Fe_{1.2}O_4$ and $FeCoFe_2O_4$ samples.

1. Introduction

Recently, the preparation of nanoparticles with difference in size becomes more for researchers and scientist worldwide (Manikandan et al., 2014; Amir et al., 2015). Many researchers have reported the new development of nanoscale crystalline ferrites considered as very suitable materials for electrical devices such as electric generators, microwave devices, transformers, and storage devices due to their strange optical, magnetic, and dielectric behavior (Sathishkumar et al., 2010).

---

[*] Corresponding author at: Department of Bio & Nanotechnology Engineering, Istanbul University, İstanbul, Turkey.
E-mail addresses: mdamir01031001@gmail.com, mda.fatih@gmail.com (Md. Amir).

Peer review under responsibility of King Saud University.

ELSEVIER Production and hosting by Elsevier

http://dx.doi.org/10.1016/j.arabjc.2016.10.010
1878-5352

Please cite this article in press as: Amir, M. et al., Oleylamine surface functionalized $FeCo_yFe_{2-y}O_4$ ($0.0 \leqslant y \leqslant 1.0$) nanoparticles. Arabian Journal of Chemistry (2016), http://dx.doi.org/10.1016/j.arabjc.2016.10.010

In recent years, inorganic and organic hybrid magnetic nanocomposites have been intensely investigated because they have unusual magnetic, optical, thermal and electrical properties (Grosso et al., 2011). Erdemi et al. tried to prepare TEG@$MnFe_2O_4$ (Triethylene Glycol@ $MnFe_2O_4$) magnetic nanocomposite via a simple polyol route (Erdemi and Baykal, 2015). Durmus et al. synthesized the polyaniline (PANI)–Mn_3O_4 magnetic nanocomposite by sonochemical method (Durmus et al., 2011). Nisar et al. reported the preparation of polyethylene based magnetic nanocomposites (Nisar et al., 2016). Yuan et al. reported the mesoporous $CoFe_2O_4$-containing silica magnetic nanocomposites (Yuan et al., 2013). Since a decade, Oleylamine coating/capped-metal oxide magnetic nanocomposites have been studied by many researchers due to its physiochemical properties which makes them a very useful materials for technological applications such as photovoltaic cell, catalyst, and semi conductors (Khan et al., 2014; Wu and Zheng, 2013; Malik, 2013). These coating are not only to protect the magnetic nanoparticles, but also to provide a new platform for further functionalization that enhances the properties of the MNPs and give a clear size and shape information of this nanoparticles. Organic solvents such as polyethylene glycol, Oleylamine (Oam), triethylene glycol, oleic acid, diethylene glycol are very efficient for the synthesis of several types of metallic, metal-oxide and semiconductor nanostructures (Mourdikoudis and Marzan, 2013; Xu et al., 2009).

So far, many studies have been done on the preparation of M^{2+} or M^{3+} substituted Fe_3O_4 nanoparticles. Amighian et al. (2013) investigated the effect of Mn^{2+} substitution on magnetic properties of Fe_3O_4 nanoparticles prepared by coprecipitation method. The microstructure and magnetotransport properties of Cu doped Fe_3O_4 films were investigated by Tripathy et al. (2008). Giri et al. (2008) investigated the biomedical applications of water based ferrofluids of substituted ferrites [$Fe_{1-x}B_xFe_2O_4$, (B = Mn, Co), (x = 0–1)]. Amir et al. (2015) studied the synthesis and electrical property investigation of Mn^{3+} substituted Fe_3O_4 nanoparticles via polyol route. Güner et al. (2015) studied Magneto-optical properties of Mn^{3+} substituted Fe_3O_4 nanoparticles. Amir et al. presented the Magneto-optical and electrical properties of $FeB_xFe_{2-2x}O_4$ nanoparticles (Amir et al., 2015a, 2015b) and electrical Properties of Cu Substituted Fe_3O_4 nanoparticles (Amir et al., 2016). Kumari et al. (2014) studied the synthesis and dielectric properties of Cr^{3+} substituted Fe_3O_4 nanoparticles. Varhney and Yogi (2014) tried to investigate the electrical transport properties of $Zn_xFe_{3-x}O_4$.

In this study, $FeCo_yFe_{2-y}O_4$ @OAm NCs were prepared by polyol route for the first time and the effect of Co^{3+} substitution and oleylamine (OAm) coating on Fe_3O_4 magnetic properties was investigated and their cation distribution and Mössbauer analyses of the products were also presented.

2. Synthesis

2.1. Materials and instrumentations

All the chemicals, Cobalt(III) acetylacetonate (99.99% trace metals), Iron(II) acetylacetonate, Iron(III) (99.95% trace metals basis) and Oleylamine (technical grade, 70%) were received from Merck and used as received.

To investigate the nature of the chemical bonds formed in the final products, Perkin Elmer BX FT-IR infrared spectrometer was used in the range of 4000–400 cm^{-1}.

The crystalline structure of $FeCo_yFe_{2-y}O_4$@OAm NCs was detected by X-ray diffraction measurements (XRD) of Rigaku D/Max—IIIC with Cu Kα, in the 2θ range of 20–70°.

Scanning Electron Microscopy (SEM) analysis was performed using FEI XL40 Sirion FEG Digital Scanning Micro-

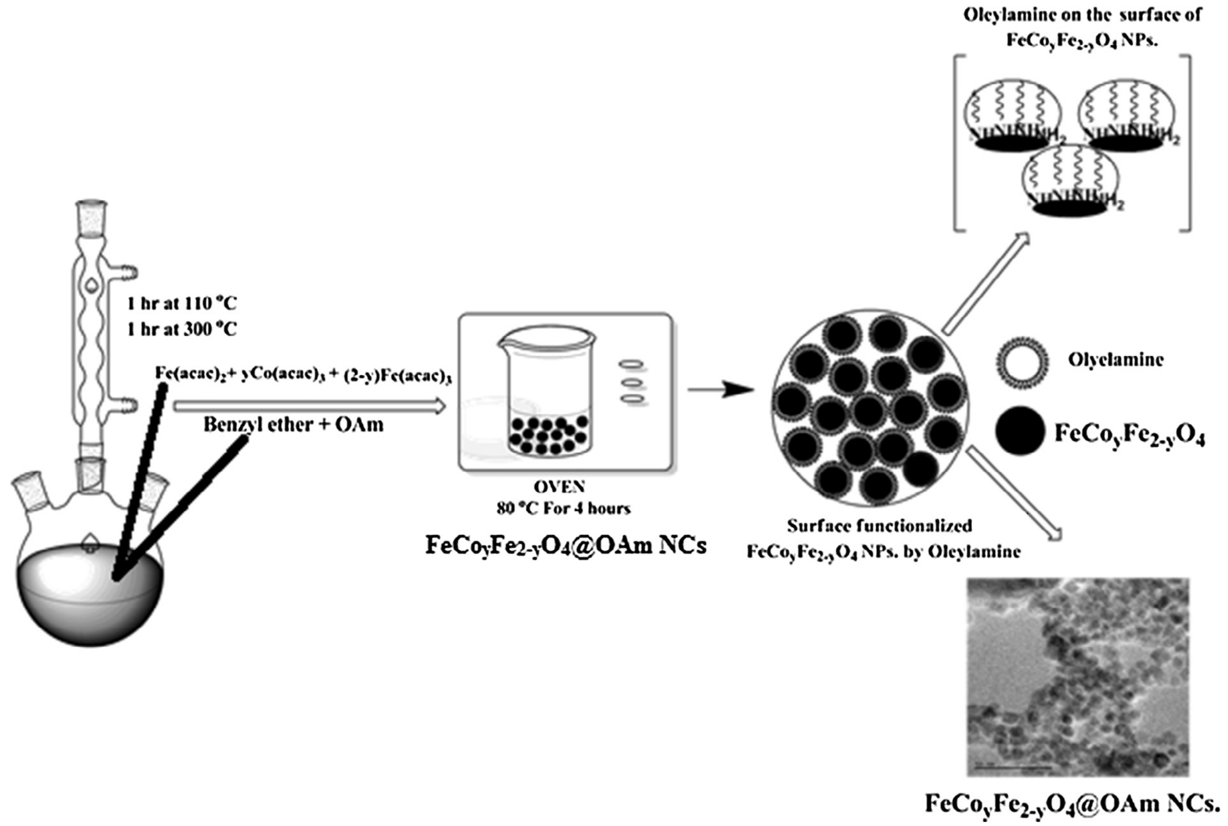

Scheme 1 Schematic representation of synthesis.

Please cite this article in press as: Amir, M. et al., Oleylamine surface functionalized $FeCo_yFe_{2-y}O_4$ ($0.0 \leqslant y \leqslant 1.0$) nanoparticles. Arabian Journal of Chemistry (2016), http://dx.doi.org/10.1016/j.arabjc.2016.10.010

scope. Samples were coated with gold at 10 mA for 2 min prior to SEM analysis.

Additionally the surface morphology of the $FeCo_yFe_{2-y}O_4$@OAm NCs was done by Transmission electron microscopy (TEM) analysis using a FEI Tecnai G2 Sphera microscope. A drop of diluted sample in alcohol was dripped on the TEM grid.

For TG analysis, Perkin Elmer Instruments model, STA 6000 instrument was used to get the information of thermal stability of $FeCo_yFe_{2-y}O_4$@OAm NCs. It was recorded under nitrogen gas atmosphere in the temperature range of 30–750 °C (10 °C/min).

Vibrating sample magnetometer (LDJ Electronics Inc. Model 9600) was used for VSM measurements and the magnetic characterization of $FeCo_yFe_{2-y}O_4$@OAm NCs was carried out at room temperature in an external field up to 15 kOe.

The 25 mCi ^{57}Co (Rh matrix) radiation source in transmission geometry was used to record the Mössbauer spectra of $FeCo_yFe_{2-y}O_4$@OAm NCs at room temperature. Moreover, Wissel velocity drive was applied and α-Fe was used to calibrate the speed scale which was performed with laser interferometry. Well-known Win-Normos least squares fitting programs were used to get the Mössbauer spectra and were fitted by the least square method. The quality of this data fitting was investigated by the χ^2-test.

2.2. Procedure

For typical synthesis of $FeCo_yFe_{2-y}O_4$@OAm NCs ($0.0 \leqslant y \leqslant 1.0$) nanocomposites, stoichiometric amounts of metal acetylacetonates $(Fe(acac)_3$, $Fe(acac)_2$ and $Co(acac)_3)$ were dissolved slowly with 15 ml OAm into a glass flask of

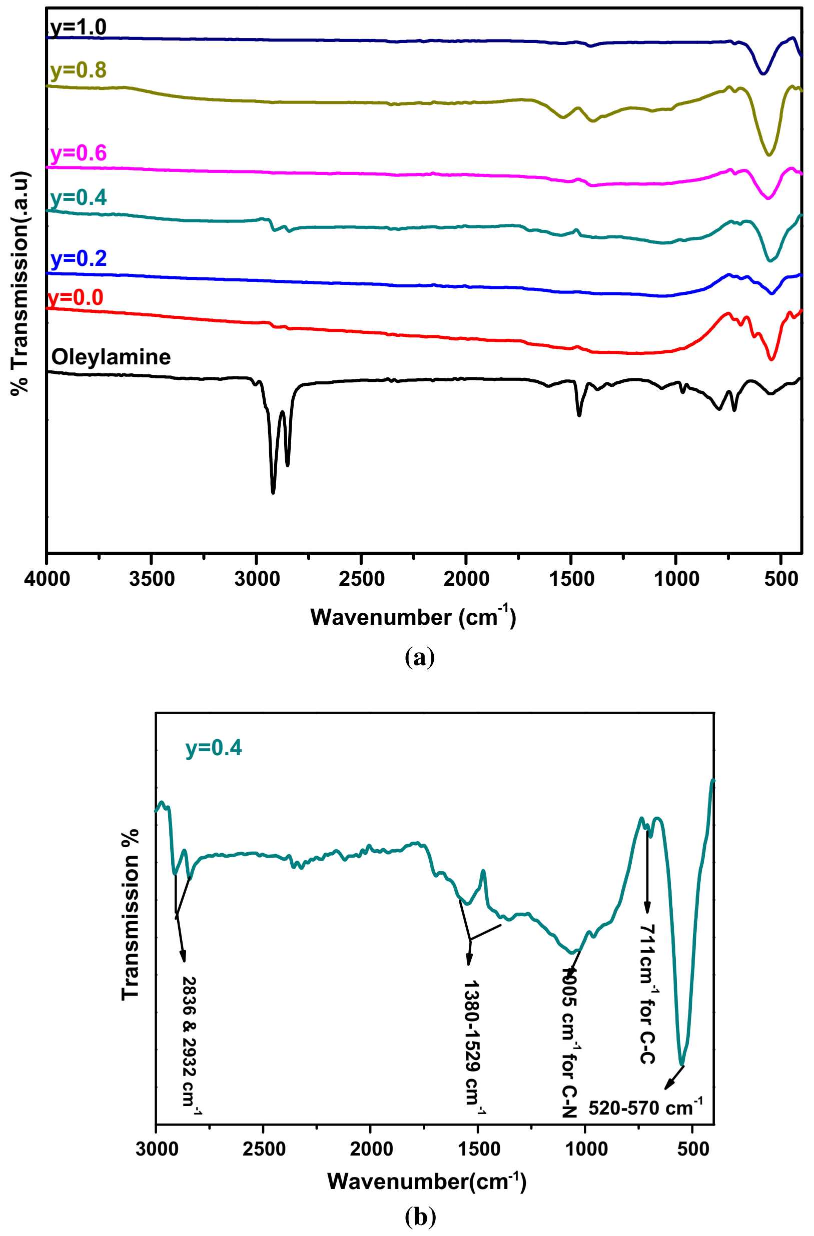

(a)

(b)

Figure 1 (a) FT-IR spectra of $FeCo_yFe_{2-y}O_4$@OAm ($0.0 \leqslant y \leqslant 1.0$) NCs and (b) FT-IR spectra of $FeCo_{0.4}Fe_{1.6}O_4$@OAm ($y = 0.4$).

Please cite this article in press as: Amir, M. et al., Oleylamine surface functionalized $FeCo_yFe_{2-y}O_4$ ($0.0 \leqslant y \leqslant 1.0$) nanoparticles. Arabian Journal of Chemistry (2016), http://dx.doi.org/10.1016/j.arabjc.2016.10.010

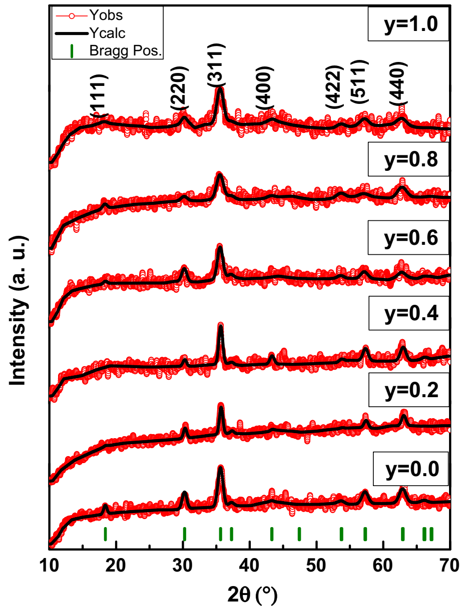

Figure 2 XRD powder patterns with Rietveld analysis for $FeCo_yFe_{2-y}O_4$@OAm ($0.0 \leqslant y \leqslant 1.0$) NCs.

three neck. Then solution was refluxed at two different temperatures, first at 110 °C for 60 min and then second was done at 300 °C for 1 h under Ar gas. Then dark brown products were taken out by simple permanent magnet. After that it was washed by solvent like ethanol three times and then dried at 80 °C for 4 h (Scheme 1).

3. Results and discussion

3.1. Infrared analysis

FT-IR spectrum of $FeCo_yFe_{2-y}O_4$@OAm NCs ($0.0 \leqslant y \leqslant 1.0$) is presented in Fig. 1 which confirmed that 1380–1529 cm^{-1} bands are due to the presence of NH_2 bending mode of OAm, and similarly the bands around 2836 and 2932 cm^{-1} are for methyl stretching (Xu et al., 2009; Niasari et al., 2009) and the peaks at 711 cm^{-1} for C–C and 1005 cm^{-1} belong to the C–N bending vibration (Özkaya et al., 2009). Moreover, a main broad metal-oxygen typical stretching modes are also observed between 520 and 570 cm^{-1} which attributed the formation of spinel ferrites (Özkaya et al., 2009). Thus, based on FT-IR results, we deduce that $FeCo_yFe_{2-y}O_4$@OAm NCs are successfully capped by oleylamine.

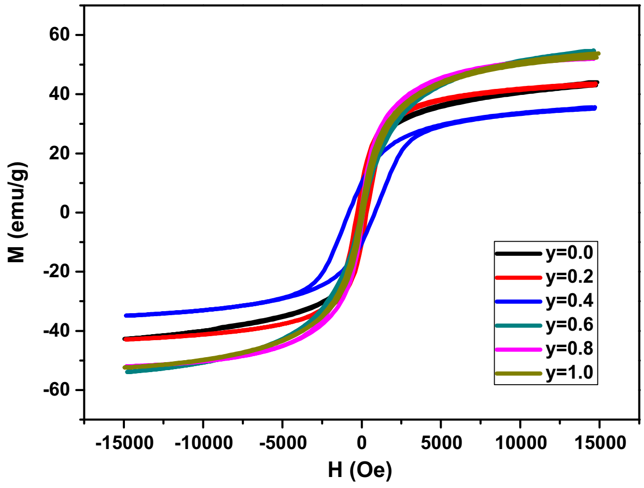

Figure 3 Plot of specific magnetization as function of $1/H^2$ of $FeCo_yFe_{2-y}O_4$@OAm ($0.0 \leqslant y \leqslant 1.0$) NCs.

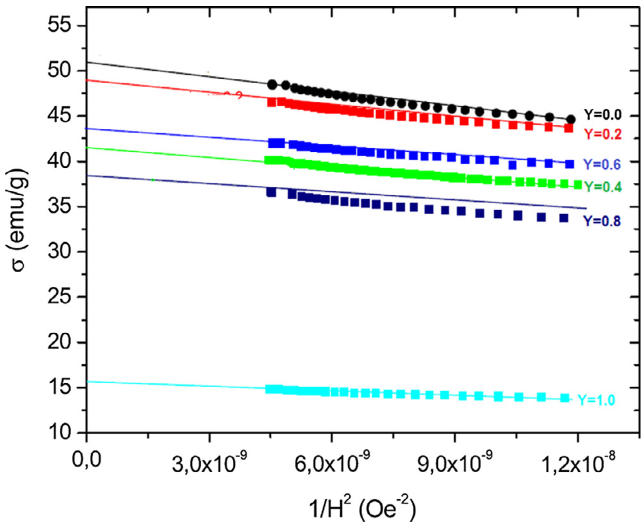

Figure 4 The room temperature M-H hysteresis curves of $FeCo_yFe_{2-y}O_4$@OAm ($0.0 \leqslant y \leqslant 1.0$) NCs.

3.2. XRD analysis

XRD powder patterns with Rietveld analysis for $FeCo_yFe_{2-y}O_4$@OAm NCs ($0.0 \leqslant y \leqslant 1.0$) NCs presented in Fig. 2 confirmed that all products have cubic spinel structure consistent with Fe_3O_4 ICDD card no. 19-629. The low crystallinity of all products revealed the nanoscale product

Table 1 Co content, refined structural parameters for $FeCo_yFe_{2-y}O_4$@OAm ($0.0 \leqslant y \leqslant 1.0$) NCs with space group Fd-3m (No. 227).

Co content (y)	A (Å)	V $(Å)^3$	Crystallite size (nm) ± 0.05	χ^2 (chi^2)	R_{Bragg}
0.0	8.359(1)	584.0(8)	17.1	0.96	9.9
0.2	8.337(5)	579.5(8)	11.7	0.95	17.3
0.4	8.351(9)	582.5(8)	21.7	1.11	33.0
0.6	8.378(3)	588.1(2)	10.7	0.99	15.9
0.8	8.369(6)	586.2(9)	7.1	0.88	22.4
1.0	8.373(9)	587.2(0)	7.3	0.89	17.0

Please cite this article in press as: Amir, M. et al., Oleylamine surface functionalized $FeCo_yFe_{2-y}O_4$ ($0.0 \leqslant y \leqslant 1.0$) nanoparticles. Arabian Journal of Chemistry (2016), http://dx.doi.org/10.1016/j.arabjc.2016.10.010

Table 2 Magnetic parameters of $FeCo_yFe_{2-y}O_4$@OAm ($0.0 \leqslant y \leqslant 1.0$) NCs.

Co^{3+} concentration (y)	Ms (emu/g)	Hc (Oe)	D_{mag} (nm)
0.0	44	275	19.97
0.2	44	290	14.25
0.4	36,8	820	23.31
0.6	61,3	60	15.37
0.8	52,2	60	14.10
1.0	56,1	60	13.67

formation for all substitutions (Ünal et al., 2010). Rietveld analyses were done by using the following *hkl* values (111), (220), (311), (400), (422), (511), and (440) (Ünal et al., 2010). The average crystallite sizes (t) were calculated based on 311 peak using Scherrer's equation.

The Co content and refined structural parameters for $FeCo_yFe_{2-y}O_4$@OAm NCs ($0.0 \leqslant y \leqslant 1.0$) NCs with space group Fd-3m are tabulated in Table 1.

3.3. VSM analysis

The room temperature M-H hysteresis curves of $FeCo_yFe_{2-y}O_4$@OAm NCs ($0.0 \leqslant y \leqslant 1.0$) NCs are given in Fig. 3. The saturation magnetization of all products was determined by intersection of the hysteresis curve with $1/H^2$ axis as $1/H^2$ approaches to zero. These magnetizations are not the saturation (ss) values of powder samples. σ_s for each sample was estimated by Stoner-Wohlfarth (S-W) model by extrapolating s vs $1/H^2$ plot to $1/H^2$ approaches zero (Sanchez-De Jesus et al., 2014; Kojima and Wohlfarth, 1982). The S-W model applies for non-interacting, single domain structures. The plot of magnetization as a function of $1/H^2$ is given for each $y = 0.0$ and CoyFe1_yFe$_2$O$_4$@OAm nanocomposite sample in Fig. 4. It can be seen in Fig. 4, the estimated σ_s magnitudes vary between minimum of 36.8 emu/g and maximum of 61.3 emu/g. Magnetization decreases with increasing Co^{3+} content at different magnitudes. The saturation magnetization of the sample having minimum Co^{3+} concentration (i.e. $y = 0.2$) is significantly lower than that of the pure Fe_3O_4 NPs which is nearly 76.5 emu/g (Lee et al., 1998). This substantial decrease in Ms can be due to the adsorption of Oleylamine molecules to the surface of Fe_3O_4 NPs through oxygen ions which have an important role in super exchange interaction between Fe^{3+} and Fe^{2+} ions. This weakens interlayer super exchange interaction (J_{AB}) Fe^{3+} - O^{2-}- Fe^{2+} which gives rise to a decrease in Ms. When Co^{3+} ions were substituted to the Fe_3O_4, Ms continued to decrease up to Co^{3+} content of $y = 0.4$. It was reported that Co^{3+} ions prefer to replace Fe^{2+} ions on octahedral side up to some concentration (Ahmed et al., 2010). The smaller ionic radii of the Co^{3+} ions (0.78 Å) disturb the J_{AB} exchange interaction diminishing the magnetization of B-sublattice (i.e., M_B). As a result, the net magnetization of Fe_3O_4 NPs decreases. Further increase of Co^{3+} concentration to $y = 0.6$ increased Ms from 36.8 emu/g to 61.3 emu/g which is a consequence of a decrease in M_A due to the replacement of the substituted ions with Fe^{2+} ions on tetrahedral side. Our Mössbauer analysis also confirmed that Co^{3+} ions replace the Fe^{2+} ions on tetrahedral sites when $y \geqslant 0.6$.

The coercive field of $FeCo_yFe_{2-y}O_4$@OAm NCs ($0.0 \leqslant y \leqslant 1.0$) NCs increases significantly when Co^{3+} concentration becomes $y = 0.4$. In general, this may happen when shape anisotropy or magnetocrystalline anisotropy of the particles is improved. All the samples have been prepared through the same preparation method and under the same conditions. Therefore, it is reasonable to think that shape anisotropy of the particles nearly the same. On the other hand, it is well known that $CoFe_2O_4$ has the largest positive anisotropy due to the strong spin-orbit coupling at Co^{3+} sites. Hence, substitution of Co^{3+} ions in magnetite increases the magnetocrystalline anisotropy of the $FeCo_yFe_{2-y}O_4$@OAm NCs ($0.0 \leqslant y \leqslant 1.0$) NCs, and thus, coercive field increases (Zhu et al., 2013). However, the presence of excess amount of Co^{3+} ions (i.e. $y \geqslant 0.6$) in magnetite lattice decreases the coercivity again, and it was calculated at Table 2.

We also performed theoretical (Langevin) fit studies for superparamagnetic data. The equations for Langevin fit studies were given in the previous reports of our research group (Baykal et al., 2015a, 2015b). The σ_s, statistical median (dm), the geometric standard deviation (Δ) are the fit parameters and they are given with average magnetic particle diameter (D_{mag}) in Table 2.

3.4. TG analysis

The content of organic OAm in $FeCo_yFe_{2-y}O_4$@OAm NCs ($0.0 \leqslant y \leqslant 1.0$) NCs was determined by TGA and three selected compositions of $y = 0.2$, $y = 0.6$ and 1.0 were taken for the TGA analysis. As shown in Fig. 5, the weight loss from RT to 150 °C is due to the loss of absorbed residual water for nanocomposites. Up to the temperature of 500 °C TG curves of all three composition showed the degradation of organic backbone of Oleylamine groups grafted to the $FeCo_yFe_{2-y}O_4$ surface and above this temperature, the weight loss for Oleylamine is almost zero which confirmed the presence of only inorganic content of $FeCo_yFe_{2-y}O_4$ ($0.0 \leqslant y \leqslant 1.0$) NPs (Kurtan et al., 2016). Thus the percent of organic content in

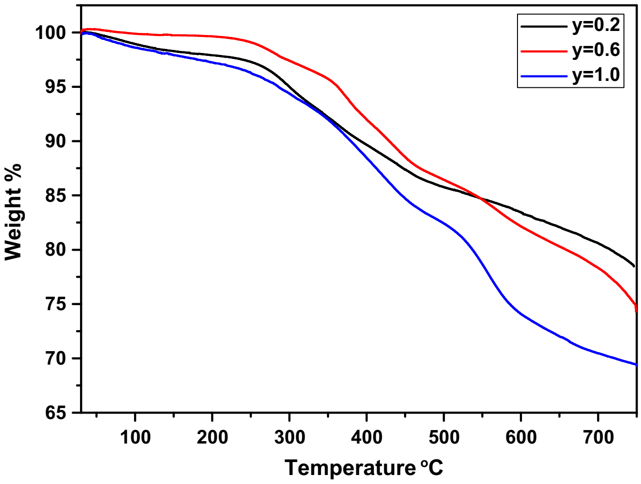

Figure 5 TG analysis of $FeCo_yFe_{2-y}O_4$@OAm ($0.0 \leqslant y \leqslant 1.0$) NCs for $y = 0.2$, $y = 0.6$ and $y = 1.0$ substitutions.

Please cite this article in press as: Amir, M. et al., Oleylamine surface functionalized $FeCo_yFe_{2-y}O_4$ ($0.0 \leqslant y \leqslant 1.0$) nanoparticles. Arabian Journal of Chemistry (2016), http://dx.doi.org/10.1016/j.arabjc.2016.10.010

three selective compositions of $y = 0.2$, $y = 0.6$, and $y = 1.0$ was estimated as ~21.60%, ~25.28%, and ~30.51% and the percentage of inorganic content ~78.40, ~74.72, ~88 and ~69.49 belonged to $FeCo_yFe_{2-y}O_4$@OAm NCs respectively. D_{mag} were also specified as 14.25 nm and 15.37 of 13.67 nm for $y = 0.2$ $y = 0.6$ and $y = 1.0$ respectively. These value are in accordance with the crystallite sizes 11.7 nm, 10.7 nm and 7.3 nm obtained from XRD analysis respectively. Therefore the TG thickness was calculated as 2.55 nm, 4.67 nm and 6.37 nm for $y = 0.2$ $y = 0.6$ and $y = 0.8$ $FeCo_yFe_{2-y}O_4$@OAm NCs respectively.

3.5. SEM analysis

SEM micrographs with their related EDX spectra and elemental maps of $FeCo_{0.2}Fe_{1.8}O_4$@OAm and $FeCo_{0.8}Fe_{1.2}O_4$@OAm nanocomposites are presented in Fig. 6a and b respectively. Uniformity in size and shape of all the compositions of $FeCo_yFe_{2-y}O_4$@OAm NCs ($0.0 \leqslant y \leqslant 1.0$) NCs was obtained by the polyol route and can be observed in SEM images. $FeCo_yFe_{2-y}O_4$@OAm NCs ($0.0 \leqslant y \leqslant 1.0$) NCs consisted of regular shaped spherical nanoparticles having small agglomeration. The SEM analysis was done with 100 nm resolution view of particles which showed smaller crystallites size and the particles are very close to each other. EDX analysis and electro mapping were also performed to characterize elements of nanocomposites and it can be seen in that nanocomposite consists of elements such as C, N, O, Fe, Co (in both EDX and elemental maps), Fig. 6a and b also shows the representative X-ray elemental maps of all elements (C, N, O, Fe, Co) detected in energy dispersive X-ray spectroscopy for $FeCo_{0.2}Fe_{1.8}O_4$@OAm and $FeCo_{0.8}Fe_{1.2}O_4$@OAm NCs. The maps indicate fairly homogeneous elemental distributions which suggest all products are uniform.

3.6. TEM analysis

TEM micrographs and related particle size distribution diagrams of $FeCo_{0.2}Fe_{1.8}O_4$@OAm and $FeCo_{0.6}Fe_{1.4}O_4$@OAm NCs are given in Fig. 7a and b respectively. Both TEM images confirmed the spherical morphology of both products. The particle sizes of $FeCo_{0.2}Fe_{1.8}O_4$@OAm and $FeCo_{0.6}Fe_{1.4}O_4$@OAm NCs were calculated as 12.2 ± 02 and 11.0 ± 0.3 nm respectively. These results are in good agreement with the crystallite sizes (from XRD) of same products.

3.7. Cation distribution

The cation distribution in spinel ferrite can be obtained from the analysis of X-ray diffraction pattern. In the present work,

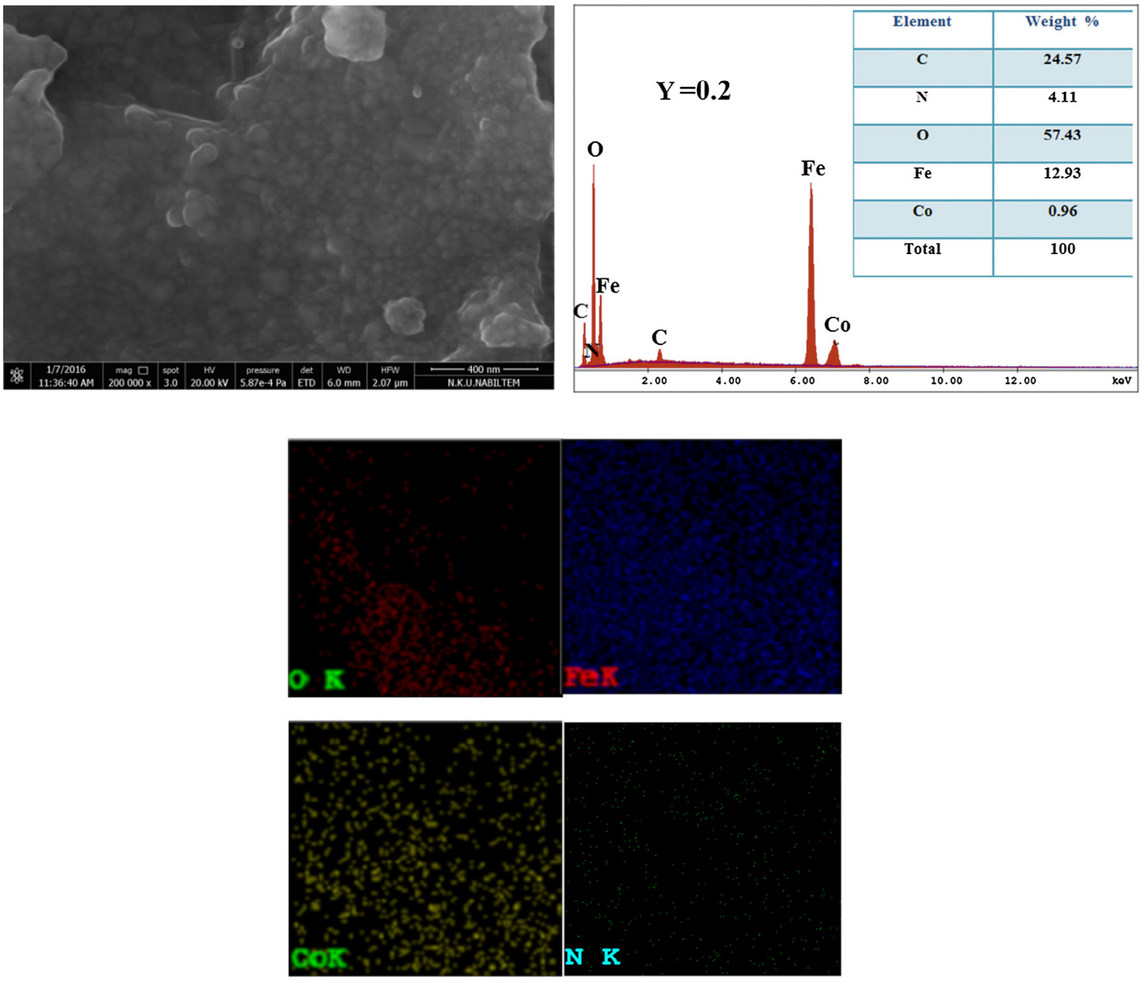

Element	Weight %
C	24.57
N	4.11
O	57.43
Fe	12.93
Co	0.96
Total	100

Figure 6 SEM micrographs with its EDX spectra of (a) $FeCo_{0.2}Fe_{1.8}O_4$@OAm and (b) $FeCo_{0.8}Fe_{1.2}O_4$@OAm NCs.

Please cite this article in press as: Amir, M. et al., Oleylamine surface functionalized $FeCo_yFe_{2-y}O_4$ ($0.0 \leqslant y \leqslant 1.0$) nanoparticles. Arabian Journal of Chemistry (2016), http://dx.doi.org/10.1016/j.arabjc.2016.10.010

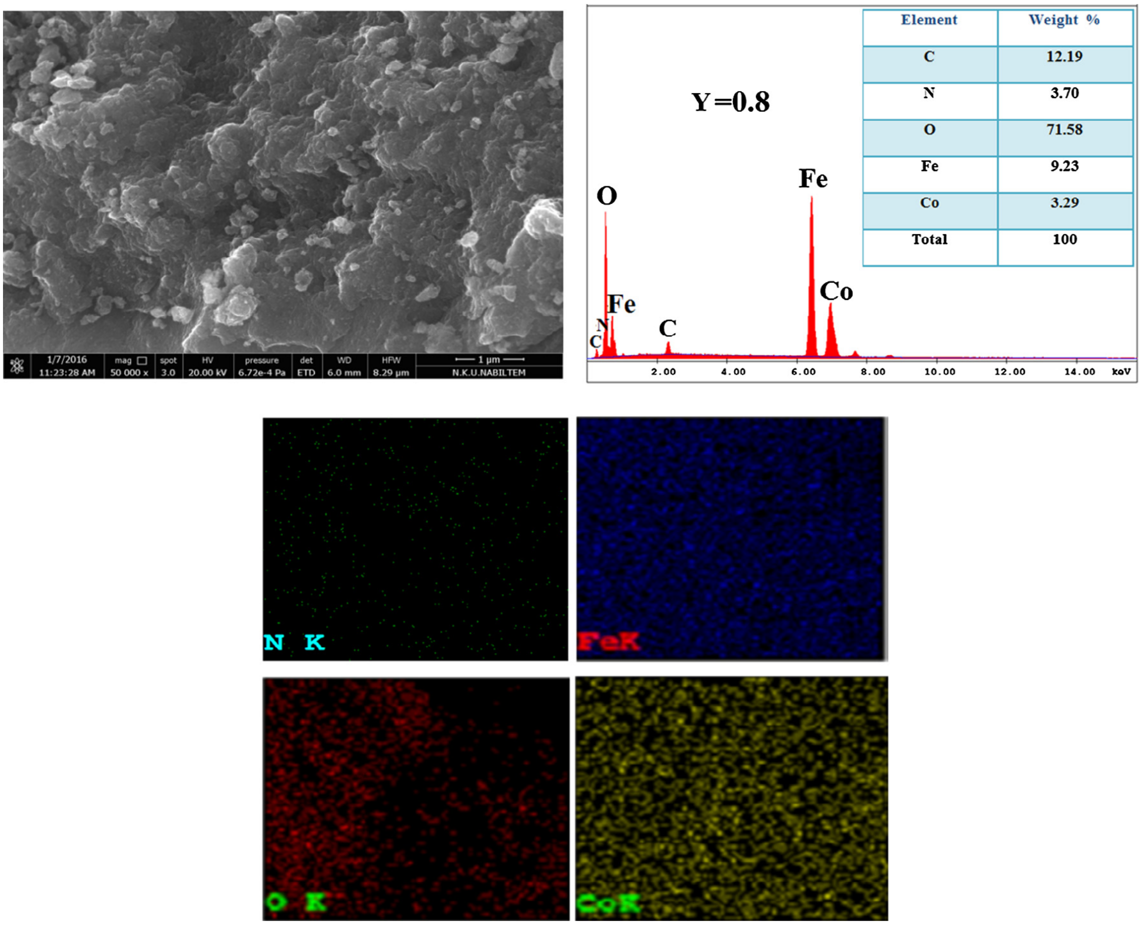

Figure 6 (*continued*)

Table 3 Cation distribution calculations of $FeCo_yFe_{2-y}O_4$@-OAm ($0.0 \leqslant y \leqslant 1.0$) NCs.

y	Tetrahedral A-site	Octahedral B-site
0.0	$Fe^{2+}_{1.0}$	$Fe^{3+}_{2.0}$
0.2	$Fe^{2+}_{1.0}$	$Co_{0.2}Fe^{3+}_{1.8}$
0.4	$Fe^{2+}_{1.0}$	$Co_{0.4}Fe^{3+}_{1.6}$
0.6	$Co_{0.1}Fe^{2+}_{0.9}$	$Fe^{2+}_{0.1}Co_{0.5}Fe^{3+}_{1.4}$
0.8	$Co_{0.2}Fe^{2+}_{0.8}$	$Fe^{2+}_{0.2}Co_{0.6}Fe^{3+}_{1.2}$
1.0	$Co_{0.3}Fe^{2+}_{0.7}$	$Fe^{2+}_{0.3}Co_{0.7}Fe^{3+}_{1.0}$

the Bertaut method (Amir et al., 2015) is used to determine the cation distribution. Ferrites are ferrimagnetic oxides with their magnetic cations forming two sublattices, namely the tetrahedral (A) and the octahedral [B] crystallographic sites.

It can be noticed in Table 3, that Fe^{2+} ions preferentially occupy tetrahedral A-site whereas Fe^{3+} ions only occupy octahedral B-site. Co^{3+} ions initially up to $y = 0.4$, only occupy octahedral B-site, as the Co^{3+} ions increased for $y > 0.4$ and it also occupies tetrahedra A-site by some fraction.

3.8. Mössbauer studies

The 57Fe Mössbauer spectra of $FeCo_yFe_{2-y}O_4$@OAm ($0.0 \leqslant y \leqslant 1.0$) NCs were done with "The 25mCi 57Co (Rh matrix) radiation source, shown in Fig. 8. The fitted spectra in Fig. 8 were used to calculate the related Mössbauer results are depicted in Table 4. The spectra were fitted using four sextets, A for the tetrahedral sites and B, B_1 and B_2 for the octahedral positions. Using the fitting computer program the B-site pattern has been fitted with three sextets. These three sextets belong to the Co^{3+} ions majorly at A-site nearest and Co^{3+} ions are nearest neighbors of the Fe at B-site.

The spectra for the sample of $FeCo_yFe_{2-y}O_4$@OAm ($0.0 \leqslant y \leqslant 1.0$) NCs with $y = 0$ showed two paramagnetic central doublets due to Fe^{3+} ions at A–site, where one of the sextets arises due to its smaller hyperfine field of the Zeeman pattern of to Fe^{3+} ions at tetrahedral (A) and the second sextet corresponds to the Fe^{3+} ions at octahedral (B) site which existed due to its larger hyperfine field of the Zeeman pattern (Amir et al., 2015; Greenwood and Gibb, 1971; Baldha and Kulkarni, 1984). The presence of paramagnetic phase C in the Mössbauer results was assumed due to the magnetically ordered spins behavior of few nearest neighbors of a fraction of Fe ions (Dobson et al., 1970; Ok et al., 1990).

The Mössbauer spectra of $FeCo_{0.6}Fe_{1.4}O_4$@OAm, $FeCo_{0.8}Fe_{1.2}O_4$@OAm and $FeCoFe_2O_4$@OAm NCs exhibit the additional presence of a quadrupole-split doublet. A fraction of Fe ions consist of few nearest neighbors possessing magnetically ordered spins are responsible for the existence of the paramagnetic phase in the Mössbauer spectra (Dobson et al., 1970). The largest hyperfine with bigger isomer shift is characteristic

Please cite this article in press as: Amir, M. et al., Oleylamine surface functionalized $FeCo_yFe_{2-y}O_4$ ($0.0 \leqslant y \leqslant 1.0$) nanoparticles. Arabian Journal of Chemistry (2016), http://dx.doi.org/10.1016/j.arabjc.2016.10.010

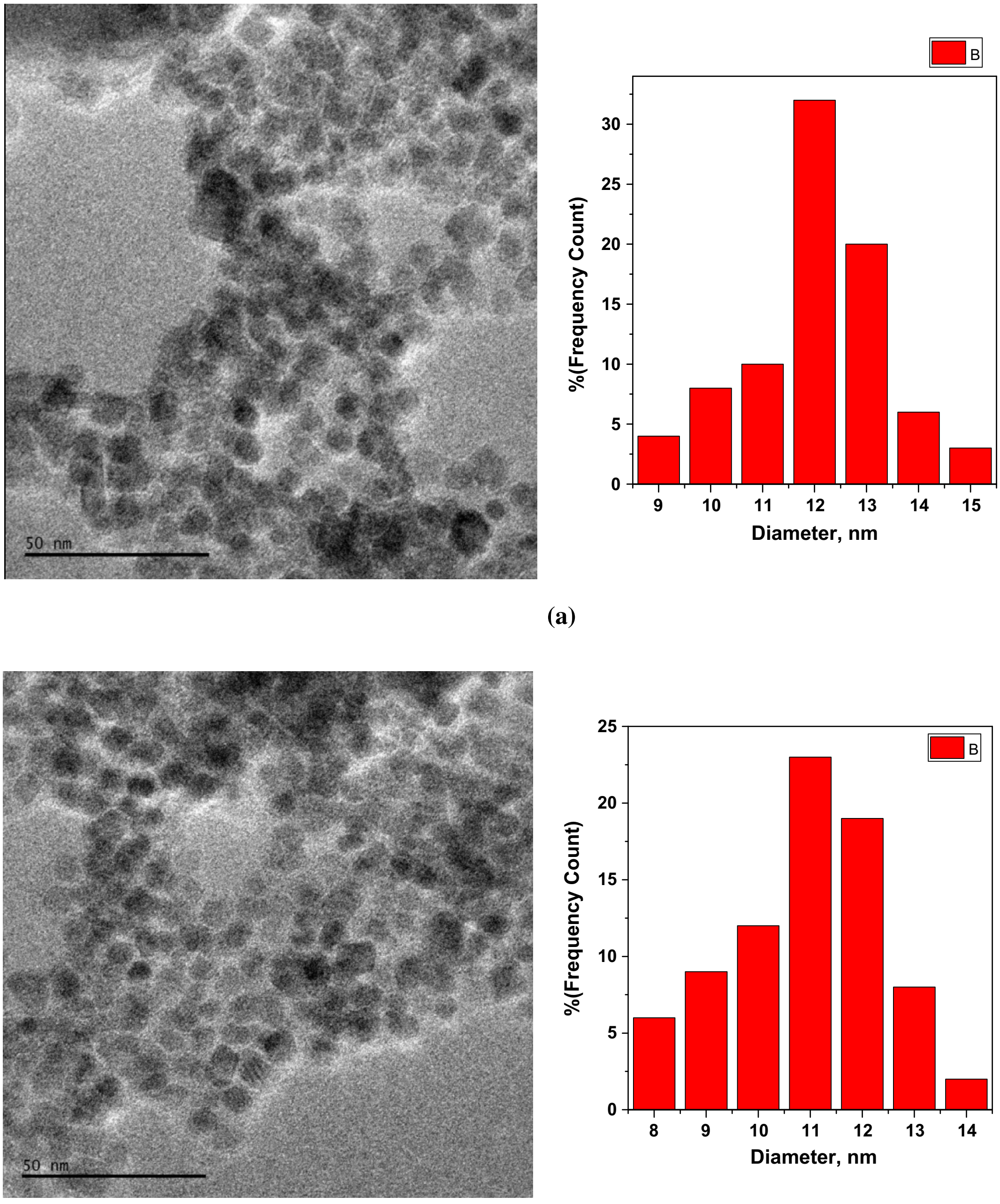

(a)

(b)

Figure 7 TEM micrographs of (a) $FeCo_{0.2}Fe_{1.8}O_4$@OAm and (b) $FeCo_{0.6}Fe_{1.4}O_4$@OAm NCs along with their particle size distribution diagrams.

of Fe^{3+} ions in the octahedral B-site but the lower values of both parameters are due to Fe^{3+} ions in the tetrahedral A site (Widatallah et al., 2013; Siddique and Butt, 2010; Jadhav et al., 2015). This is because of the presence of magnetic ion (Co^{3+}) at B-site (Jadhav et al., 2015). In most of the magnetic materials such as magnetite and ferrites, hyperfine magnetic field at B-site is generally considered to be larger than hyperfine magnetic field of that A-site and this corresponds to the dipolar field. This hyperfine behavior of A-site and B-site is due to deviation from covalent nature and cubic symmetry of tetrahedral bonds (Widatallah et al., 2013; Siddique and Butt, 2010; Jadhav et al., 2015; Lakshman et al., 2006).

According to Table 4, as the concentration of Co^{3+} ions increases, the hyperfine field values at B- and A- sites slowly decrease which can be explained by Neel's super exchange interaction model (Neel, 1948). Neel's model is based on the inter sublattice exchange interactions. From the Mössbauer spectra, it can be said that both A and B sites are occupied by Fe^{3+} and Co^{3+} ions, and mostly: $Fe^{3+}_A - O - Fe^{3+}_B$, $Fe^{3+}_A - O - Co^{3+}_B$, $Fe^{3+}_B - O - Co^{3+}_A$ interactions can be taken under consideration, as the interaction of AA or BB assumed to be very weak and can be neglected. Therefore only strong interaction can originate the net magnetic field. As the concentration of larger number Co^{3+} ions of lower magnetic moment

Please cite this article in press as: Amir, M. et al., Oleylamine surface functionalized $FeCo_yFe_{2-y}O_4$ ($0.0 \leqslant y \leqslant 1.0$) nanoparticles. Arabian Journal of Chemistry (2016), http://dx.doi.org/10.1016/j.arabjc.2016.10.010

Table 4 Parameters of Mössbauer spectra of $FeCo_yFe_{2-y}O_4$@OAm ($0.0 \leqslant y \leqslant 1.0$) NCs ($B_{hf}$: hyperfine magnetic field. I.S: isomer shift. Q.S: quadrupole splitting. *W*: line width. R_A: Relative area).

x	Spectral component	I.S. (±0.003) (mm s^{-1})	Q.S. (±0.005) (mm s^{-1})	H_{hf} (±0.02) (T)	*W* (±0.0) (mm s^{-1})	Area (%)
0.2	Sx- B: Fe^{3+}	0.3433	−0.0061	50.862	0.38293	17.023
	Sx- A: Fe^{3+}	0.3097	0.0115	49.522	0.3584	18.51
	Sx- B_1: Fe^{3+}	0.3245	−0.0252	47.872	0.5651	30.353
	Sx- B_2: Fe^{3+}	0.4046	−0.003	44.223	1.5042	34.114
0.4	Sx- B: Fe^{3+}	0.3441	−0.051	50.525	0.357	15.152
	Sx- A: Fe^{3+}	0.2863	0.0325	49.205	0.3591	25.024
	Sx- B_1: Fe^{3+}	0.3652	−0.0647	47.879	0.5336	17.036
	Sx- B_2: Fe^{2+}, Fe^{3+}	0.5152	0.0248	45.183	0.7155	42.788
0.6	Sx- B: Fe^{3+}	0.3304	0.0026	49.445	0.3578	15.622
	Sx- A: Fe^{3+}	0.3159	−0.0016	47.382	0.6122	16.316
	Sx- B_1: Fe^{3+}	0.3366	−0.0064	44.793	0.6424	19.29
	Sx- B_2: Fe^{3+}	0.3497	0.0181	40.22	1.241	31.349
	Db: Fe^{3+}	0.3469	1.413	–	1.9849	17.422
0.8	Sx- B: Fe^{3+}	0.3312	0.0212	48.636	0.7188	12.152
	Sx- A: Fe^{3+}	0.3189	0.02125	45.36	0.6795	17.094
	Sx- B_1: Fe^{3+}	0.3209	−0.03267	40.204	2.2493	53.939
	Db: Fe^{3+}	0.3403	1.1717	–	1.4256	16.816
1	Sx- B: Fe^{3+}	0.3236	0.0174	48.458	0.7375	12.62
	Sx- A: Fe^{3+}	0.3316	−0.005	45.901	0.7468	23.486
	Sx- B_1: Fe^{3+}	0.3519	−0.0466	41.92	2.2965	46.762
	Db: Fe^{3+}	0.3339	0.6525	–	1.2037	17.131

of 5.4 μ_B increased, Fe^{3+} ions of higher magnetic moment of 5.92 μ_B replaced by the Co^{3+} ions and the number of magnetic linkages in $Fe_A^{3+} - O - Fe_B^{3+}$, $Fe_A^{3+} - O - Co_B^{3+}$ and $Fe_B^{3+} - O - Co_A^{3+}$ decrease and consequently Fe^{3+} nuclei experience a fraction of reduction in the magnetic field at both the sub lattices.

The chemical isomer shifting (I.S) normally takes place due to the change in differing chemical environments and nuclear radius and depends on s-electron density and the shielding effect of p, d and f electrons. As it can be seen in Mössbauer spectra, the isomer shift at B sites is larger than that of A-sites, due to the higher covalence which resulted in the larger overlapping of Fe^{3+}–O^{2-} ions at B-sites as compared to A-site (Lakshman et al., 2006). The observed and calculated ranges of isomer shift of the A and B magnetic pattern are 0.2863–0.5152 mm s^{-1} at room temperature. It is well known that in the magnetically ordered phase, the valence of Fe should be mainly distinguished by the isomer shift (0.6–1.7 mm s^{-1} for Fe^{2+}, 0.05–0.5 mm s^{-1} for Fe^{3+} and −0.15 to 0.05 mm s^{-1} for Fe^{4+}) (Hodges et al., 2000). Thus the isomer shift values attribute to Fe^{3+} charge state behavior in A and B sites, and are specific characteristics of the high spin Fe^{3+} charge state. The high values of isomer shift of B_2 of $FeCo_yFe_{2-y}O_4$@OAm ($0.0 \leqslant y \leqslant 1.0$) NCs for $y = 0.4$ may signal the presence of Fe^{2+} ions at B sites. The Mössbauer study suggested that isomer shift values do not change as the concentration of Co^{3+} ions varies, which explained that there is no specific change in s-electron charge distribution around the Fe^{3+} nucleus at A or B sites depending on concentrations of Co^{3+} ions.

In Table 4, Q.S value was calculated for all the compositions of $FeCo_yFe_{2-y}O_4$@OAm ($0.0 \leqslant y \leqslant 1.0$) NCs. This value gives the information regarding the local distortions and symmetry of crystal lattice. The electric field gradient (EFG) of varying magnitude, sign, direction and symmetry causes due to the nonspherical distribution of 3d electrons of the cations and effective charge on the neighboring ions (Ata- Allah et al., 2000). Siddique et al. also reported that the ionic radii play a large role than their charges in the local symmetry of EFG (Siddique and Butt, 2010). The values of Q. S for observed components with respect to composition of $FeCo_yFe_{2-y}O_4$@OAm ($0.0 \leqslant y \leqslant 1.0$) NCs are negligible and change randomly with addition *y* value.

4. Conclusion

In this study, single spinel phase $FeCo_yFe_{2-y}O_4$@OAm ($0.0 \leqslant y \leqslant 1.0$) NCs were prepared via polyol method. Nanosize structure and morphology of as prepared nanocomposites were confirmed using XRD powder diffraction, SEM micrographs and TEM images. EDX analyses confirmed the predicted chemical composition of the products. Nearly homogeneous distribution of elements in products was confirmed by Elemental mapping. The successful surface modification of Fe_3O_4 NPs by capping of OAm was proved by both TG analysis and FT-IR spectroscopy respectively. Cation distribution calculations showed that octahedral and tetrahedral site preference of Fe^{2+}, Fe^{3+} and Co^{3+} ions depend on the substitution (*x*). The smaller ionic radius of Co^{3+} ions (0.78 Å) disturbs the J_{AB} exchange interaction diminishing the magnetization of B-sublattice (i.e., M_B). As a result, the net magnetization of Fe_3O_4 NPs decreases. The hyperfine fields (H_{hf}) at A and B sites decrease with increase in concentration of Co^{3+} ions. The Mössbauer spectrum is composed of ferromagnetic sextets for the samples. The superparamagnetic doublet is also formed for $y = 0.6$, 0.8 and 1 values. Cubic symmetry is not affected with concentration of Co^{3+} ions. As seen from the Mössbauer results, there is an increase in the coercivity of Fe_3O_4 NPs due to the doping of transition

Please cite this article in press as: Amir, M. et al., Oleylamine surface functionalized $FeCo_yFe_{2-y}O_4$ ($0.0 \leqslant y \leqslant 1.0$) nanoparticles. Arabian Journal of Chemistry (2016), http://dx.doi.org/10.1016/j.arabjc.2016.10.010

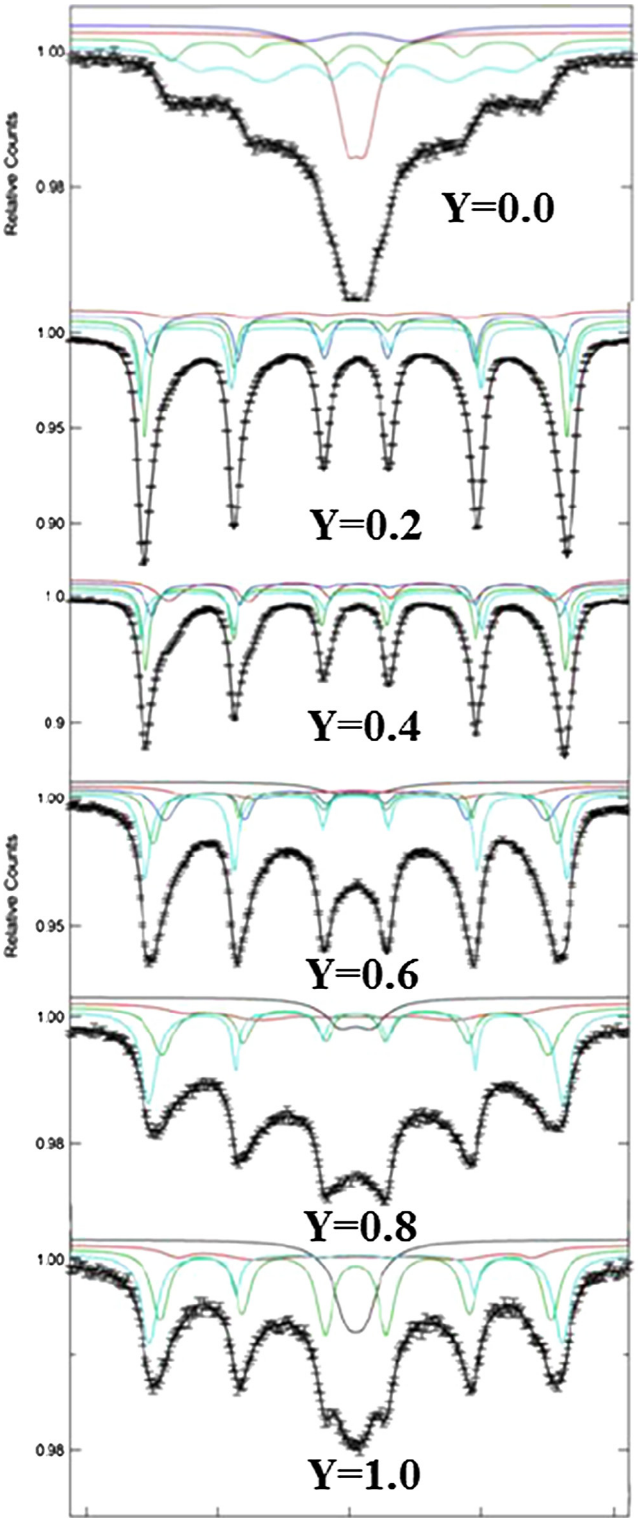

Figure 8 Room temperature Mössbauer spectra of $FeCo_yFe_{2-y}O_4$@OAm ($0.0 \leqslant y \leqslant 1.0$) NCs.

Co^{3+} ions and behavior of as prepared $FeCo_yFe_{2-y}O_4$@OAm ($0.0 \leqslant y \leqslant 1.0$). NCs can be considered to be used in recording media, magnetic fluids recording, catalysis, biotechnology/biomedicine, material sciences, photo catalysis, electrochemical and bioelectrochemical sensing, microwave absorption, magnetic resonance imaging [MRI], medical diagnosis, data storage, and environmental remediation.

Acknowledgments

Md. Amir wants to thank the Turkish Research Council (TÜBİTAK) for his PhD scholarship.

References

Ahmed, M.A., Mansour, S.F., El- Dek, S.I., 2010. Influence of Co content on the characterization and magnetic properties of magnetite. Ceram. Int. 36, 1529–1533.

Amighian, J., Karimzadeh, E., Mozaffari, M., 2013. JMMM 332, 157–162.

Amir, Md., Unal, B., Shirsath, Sagar E., Geleri, M., Sertkol, M., Baykal, A., 2015. Polyol synthesis of Mn^{3+} substituted Fe_3O_4 nanoparticles: cation distribution, structural and electrical properties. Superlattices Microstruct. 85, 747–760.

Amir, Md., Baykal, A., Güner, S., Sertkol, M., Sözeri, H., Toprak, M.S., 2015. Synthesis and Characterization of $Co_xZn_{1-x}AlFeO_4$ Nanoparticles. J. Inorg. Organomet. Polym. 25, 747–754.

Amir, Md., Geleri, M., Güner, S., Baykal, A., Sözeri, H., 2015a. Magneto optical properties of $FeB_xFe_{2-2x}O_4$ nanoparticles. J. Inorg. Organomet. Polym. 25, 1111–1119.

Amir, Md., Ünal, B., Geleri, M., Güngüneş, H., Shirsath, Sagar E., Baykal, A., 2015b. Electrical properties and hyperfine interactions of boron doped Fe_3O_4 nanoparticles. Superlattices Microstruct. 88, 450–466.

Amir, Md., Erdemi, H., Geleri, M., Baykal, A., 2016. Electrical properties of Cu substituted Fe_3O_4 nanoparticles. J. Supercond. Nov. Magn. 29, 389–400.

Ata- Allah, S., Fayek, M.K., Refai, H.S., Mostafa, M.F., 2000. Mössbauer effect study of copper containing nickel-aluminate ferrite. J. Solid State Chem. 149, 434–442.

Baldha, G.J., Kulkarni, R.G., 1984. Mössbauer study of the spinel system $Ge_xCu_{1-x}Fe_2O_4$. Solid State Commun. 49, 169–172.

Baykal, A., Güner, S., Demir, A., 2015a. Synthesis and magneto-optical properties of triethylene glycol stabilized $Mn_{1-x}Zn_x\,Fe_2O_4$ nanoparticles. J. Alloy Compd. 619, 5–11.

Baykal, A., Esir, S., Demir, A., Güner, S., 2015b. Magnetic and optical properties of $Cu_{1-x}Zn_xFe_2O_4$ nanoparticles dispersed in a silica matrix by a sol-gel auto-combustion method. Ceram. Int. 41, 231–239.

Dobson, D.C., Linnet, J.W., Rahman, M.M., 1970. Entropies of mixing of solids with a retrograde solidus. J. Phys. Chem. Solids 31, 713–727.

Dobson, D.C., Linnet, J.W., Rahman, M.M., 1970. Mössbauer studies of the charge transfer process in the system $Zn_xFe_{3-x}O_4$. J. Phys. Chem. Solids 31, 2727–2733.

Durmus, Z., Baykal, A., Kavas, H., Sözeri, H., 2011. Preparation and characterization of polyaniline (PANI)–Mn_3O_4 nanocomposite. Physica B 406, 1114–1120.

Erdemi, H., Baykal, A., 2015. Dielectric properties of triethylene glycol-stabilized $Mn_{1-x}Zn_xFe_2O_4$ nanoparticles. Mater. Chem. Phys. 165, 156–167.

Giri, J., Pradhan, P., Somani, V., Chelawat, H., Chhatre, S., Banerjee, R., Bahadur, D., 2008. JMMM 320, 724–730.

Greenwood, N.N., Gibb, T.C., 1971. Mössbauer Spectroscopy. Chapman & Hall, London, p. 259.

Grosso, D., Ribot, F., Boissiere, C., Sanchez, C., 2011. Molecular and supramolecular dynamics of hybrid organic–inorganic interfaces for the rational construction of advanced hybrid nanomaterials. Chem. Soc. Rev. 40, 829–848.

Güner, S., Amir, Md., Geleri, M., Sertkol, M., Baykal, A., 2015. Magneto-optical properties of Mn^{3+} substituted Fe_3O_4 nanoparticles. Ceram. Int. 41, 10915–10922.

Hodges, J.P., Short, S., Jorgensen, J.D., Xiong, X., Dabrovski, B., Mini, S.M., Kimball, C.W., 2000. Evolution of oxygen-vacancy ordered crystal structures in the perovskite series $\mathrm{Sr}n\mathrm{Fe}n\mathrm{O}_3n_{-1}$

Please cite this article in press as: Amir, M. et al., Oleylamine surface functionalized $FeCo_yFe_{2-y}O_4$ ($0.0 \leqslant y \leqslant 1.0$) nanoparticles. Arabian Journal of Chemistry (2016), http://dx.doi.org/10.1016/j.arabjc.2016.10.010

(n = 2, 4, 8, and ∞), and the relationship to electronic and magnetic properties. J. Solid State Chem. 151, 190–209.

Jadhav, P., Patankar, K., Mathe, V., Tarwal, N.L., Jang, Jae-Hung, Puri, V., 2015. Structural and magnetic properties of $Ni_{0.8}Co_{0.2-2x}Cu_xMn_xFe_2O_4$ spinel ferrites prepared via solution combustion route. J. Magn. Magn. Mater. 385, 160–165.

Khan, M.A., Sarker, J.C., Lee, S., Mangham, S.C., Manasreh, M.O., 2014. Synthesis, characterization and processing of cubic iron pyrite nanocrystals in a photovoltaic cell. Mater. Chem. Phys. 148, 1022–1028.

Kojima, H., Wohlfarth, E.P., 1982. Ferromagnetic Materials, vol. 3. Amsterdam, North-magneto-optical recording, Holland, p. 305.

Kumari, N., Kumar, V., Singh, S.K., 2014. Ceram. Int. 40, 12199–12205.

Kurtan, U., Güngüneş, H., Sözeri, H., Baykal, A., 2016. Synthesis and characterization of monodisperse $NiFe_2O_4$ nanoparticles. Ceram. Int. 42, 7987–7992.

Lakshman, A., Subba Rao, P.S.V., Rao, K.H., 2006. Mössbauer spectroscopic analyses of $Mg_{0.9}$ $Cu_{0.1}Mn_{0.05}Cr_xFe_{1.95-x}O_4$ spinel ferrites. Mater. Lett. 60, 7–10.

Lee, J.G., Park, J.Y., Kim, C.S., 1998. Growth of ultra-fine cobalt ferrite particles by a sol–gel method and their magnetic properties. J. Mater. Sci. 33, 3965–3968.

Malik, M.A., 2013. 4.09 - compound semiconductors: chalcogenides. In: Reedijk, Jan, Poeppelmeier, Kenneth (Eds.), Comprehensive Inorganic Chemistry II. second ed. Elsevier, Amsterdam, pp. 177–210.

Manikandan, A., Judith Vijaya, J., Arul Mary, J., John Kennedy, L., Dinesh, A., 2014. Structural, optical and magnetic properties of Fe_3O_4 nanoparticles prepared by a facile microwave combustion method. J. Ind. Eng. Chem. 20, 2077–2085.

Mourdikoudis, S., Marzan, L.M.L., 2013. Oleylamine in nanoparticle synthesis. Chem. Mater. 25, 1465–1476.

Neel, L., 1948. Ferromagnetic compounds of manganese with perovskite structure. Ann. Phys. 3, 137–198.

Niasari, M.S., Fereshteh, Z., Davar, F., 2009. Synthesis of oleylamine capped copper nanocrystals via thermal reduction of a new precursor. Polyhedron 28, 126–130.

Nisar, M., Bergmann, C., Geshev, J., Quijada, R., Galland, G.B., 2016. An efficient approach to the preparation of polyethylene magnetic nanocomposites. Polymer 97, 131–231.

Ok, H.N., Baek, K.S., Lee, H.S., Kim, C.S., 1990. Mössbauer study of $Cu_{0.5}Fe_{0.5}Cr_2S_4$. Phys. Rev. B Condens. Matter. 41, 62–64.

Özkaya, T., Toprak, M.S., Baykal, A., Kavas, H., Köseoğlu, Y., Aktaş, B., 2009. Synthesis of Fe_3O_4 nanoparticles at 100 °C and its magnetic characterization. J. Alloys Compd. 472, 18–23.

Sanchez-De Jesus, F., Bolarin-Miro, A.M., Cortes-Escobedo, C.A., Valenzuela, R., Ammar, S., 2014. Mechanosynthesis, crystal structure and magnetic characterization of M-type SrFe12O19. Ceram. Int. 40, 4033e4038.

Sathishkumar, G., Venkataraju, C., Sivakumar, K., 2010. Synthesis, structural and dielectric studies of nickel substituted cobalt-zinc ferrite. Mater. Sci. Appl. 1, 19–24.

Siddique, M., Butt, N.M., 2010. Effect of particle size on degree of inversion in ferrites investigated by Mössbauer spectroscopy. Phys. B 405, 4211–4215.

Tripathy, D., Adeyeye, A.O., Boothroyd, C.B., Shannigrahi, S., 2008. J. Appl. Phys. 103, 07F701.

Ünal, B., Durmus, Z., Baykal, A., Sözeri, H., Toprak, M.S., Alpsoy, L., 2010. L-histidine coated iron oxide nanoparticles: synthesis, structural and conductivity characterization. J. Alloy. Compd. 505, 172–178.

Varhney, D., Yogi, A., 2014. Optik 125, 6629–6633.

Widatallah, H.M., Al-Mamari, F.A.S., Al-Saqri, N.A.M., Gismelseed, A.M., Al-Omari, I.A., Al-Shahumu, T.M.H., Alhaj, A.F., Abo El Ata, A.M., Elzain, M.E., 2013. Mater. Chem. Phys. 140, 97–103.

Wu, B., Zheng, N., 2013. Surface and interface control of noble metal nanocrystals for catalytic and electrocatalytic applications. Nano Today 8, 168–197.

Xu, Z., Shen, C., Hou, Y., Gao, H., Sun, S., 2009. Oleylamine as both reducing agent and stabilizer in a facile synthesis of magnetite nanoparticles. Chem. Mater 21, 1778–1780.

Yuan, X., Cheng, L., Liu, W., Zhang, L., 2013. Synthesis of ordered mesoporous $CoFe_2O_4$-containing silica by self-assembly process. J. Magn. Magn. Mater. 331, 198–203.

Zhu, H., Zhang, S., Huang, Y.-X., Wu, L., Sun, S., 2013. Monodisperse $M_xFe_{3-x}O_4$ (M = Fe, Cu Co, Mn) nanoparticles and their electrocatalysis for oxygen reduction reaction. Nano Lett. 13 (6), 2947–2951.

Please cite this article in press as: Amir, M. et al., Oleylamine surface functionalized $FeCo_yFe_{2-y}O_4$ ($0.0 \leqslant y \leqslant 1.0$) nanoparticles. Arabian Journal of Chemistry (2016), http://dx.doi.org/10.1016/j.arabjc.2016.10.010